PERGAMON Computers and Mathematics with Applications 41 (2001) 723–734

An International Journal
computers & mathematics
with applications

www.elsevier.nl/locate/camwa

Gas-Kinetic Schemes for Compressible Flow of Real Gases

HUA-ZHONG TANG
State Key Laboratory of Scientific and Engineering Computing
Institute of Computational Mathematics
Academia Sinica
P.O. Box 2719, Beijing 100080, P.R. China
thz@lsec.cc.ac.cn

(Received April 1999; revised and accepted December 1999)

Abstract—This paper extends gas-kinetic schemes to the Euler equations for real gases. In the current scheme, the Maxwell-Boltzmann gas distribution function is modified to recover macroscopic flow equations. More specifically, the internal degree of freedom of the gas distribution function becomes a function of flow variables according to the general equation of state. The numerical results confirm the accuracy and robustness of the gas-kinetic approach. © 2001 Elsevier Science Ltd. All rights reserved.

Keywords—Euler equations, Gas-kinetic schemes, Real gas, Maxwellian distribution.

1. INTRODUCTION

The development of gas-kinetic methods for compressible flow simulations, such as the KFVS schemes and the BGK-type schemes, has become mature in the past few years. The gas-kinetic schemes have provided robust and accurate numerical solutions for various unsteady compressible flows (see [1–11]).

Numerical schemes for compressible flow of real gases have been developed by several authors in [12–19]. Colella and Glaz in [12] tried to construct an exact Riemann solution for real gases. Glaister in [13,14] presented an approximate linearised Riemann solver for the Euler equations with a general equation of state. Grossman and Walters [15], Liou *et al.* [16] and Vinokur and Montagne [17] extended the flux-vector splitting and flux-difference splitting to the Euler equations of real gases.

Most of the previous proposed methods require the exact computation of the pressure and its derivatives, such as the pressure distributions in the Riemann solver. This is expensive and problematic when there is no analytic expression of the pressure law. Recently, Coquel and Perthame [19] introduced an energy relaxation theory for the Euler equations of real gases. Their method does not need computations of derivatives of the pressure law nor a Riemann solver.

The work was supported in part by the National Natural Science Foundation of China, and in part by the foundation of National Key Laboratory of Computational Physics. The author wishes to thank Prof. Huamo Wu and Dr. Kun Xu for many interesting discussions. The author would also like to thank the referees for useful suggestions.

PII: S0898-1221(00)00316-3

In [20], Montarnal and Shu studied the combination of this relaxation method and the high-order WENO schemes for real gases. However, the robustness of their algorithm seems to depend on the way of energy decomposition.

In this paper, we will extend gas-kinetic BGK-type schemes to the simulations of the Euler equations for real gases. Here, the Maxwell-Boltzmann particle distribution function is used to recover the equations of real gases with a modification of the internal degree of freedom. This new scheme does not require a specific form of the equation of state, nor the derivatives of the pressure law. The current scheme has been applied to a one-dimensional shock reflection and three shock-tube problems for several special equations of state. The extension of the BGK-type schemes to multidimensional real gases will be presented in the future.

This paper is organized as follows. In Section 2, we recall the connection between the Boltzmann and the Euler descriptions for an ideal gas, and introduce a new local equilibrium state to recover the real gas effect. In Section 3, a high resolution BGK-type scheme is presented with the above new equilibrium distribution. Several numerical examples are presented in Section 4. Section 5 is the conclusion.

2. PRELIMINARIES

In the following, we consider compressible Euler equations in one dimension

$$\frac{\partial U}{\partial t} + \frac{\partial F(U)}{\partial x} = 0, \tag{1}$$

where

$$U = [\rho, \rho u, E]^\top \tag{2}$$

are the flow variables, and

$$F(U) = \left[\rho u, \rho u^2 + p, u(E+p)\right]^\top \tag{3}$$

the corresponding fluxes. The energy density E includes both kinetic and thermal ones,

$$E = \frac{1}{2}\rho u^2 + \rho e(x,t).$$

In the above, ρ, u, p, and e represent the density, velocity, pressure, and the specific internal energy density, respectively.

In order to close system (1), an equation of state is needed to connect ρ, e, and p, such as

$$p = p(\rho, e). \tag{4}$$

In the general case, the function $p(\cdot,\cdot)$ satisfies conditions of hyperbolicity for system (1). For an ideal gas, equation (4) becomes

$$p = (\gamma - 1)\rho e, \tag{5}$$

where γ is the ratio of specific heat capacities of the fluid. This is sometimes called a γ-gas law.

The macroscopic flow motion can also be described according to particle motion, or the statistical description of a fluid. Due to the large number of particles in small volume in a continuum regime, it is impossible to follow each one. Instead, a continuous distribution function $f(x_i, t, v_i)$ is used to describe the probability of particles to be located in a certain velocity interval. The velocity distribution function f obeys the Boltzmann equation (here we restrict to the one-dimensional case)

$$\frac{\partial f}{\partial t} + v \cdot \frac{\partial f}{\partial x} = J(f, f), \tag{6}$$

where the right-hand side represents the particle collision term, which vanishes in the Euler limit.

The thermodynamic aspect of hydrodynamical equations is based on the assumption that the departure of the gas from the local equilibrium state is sufficiently small. The equilibrium state g can be uniquely constructed once the mass, momentum, and energy densities are defined. The equilibrium state plays an important role in studying some physical properties of the fluid and the construction of gas-kinetic schemes. We refer readers to [1–11] for more detail about the construction of gas-kinetic schemes and [20,21] for the physics of kinetic theory.

For the compressible Euler equations (1) with a γ-gas law (5), the Maxwell-Boltzmann distributions for the equilibrium state is [9–11]

$$g = \rho\left(\frac{\lambda}{\pi}\right)^{(1+K)/2} e^{-\lambda\left[(v-u)^2+\xi^2\right]}, \tag{7}$$

where K is the internal degree of freedom which is related to γ,

$$K = -1 + \frac{2}{\gamma - 1}, \tag{8}$$

λ is a function of the density and pressure, such that $\lambda = \rho/2p$, and $\xi^2 = \xi_1^2 + \cdots + \xi_K^2$. The Euler equations (1) can be cast in the moment form as

$$\left\langle \Psi, \frac{\partial g}{\partial t} + v \cdot \frac{\partial g}{\partial x} \right\rangle = 0, \tag{9}$$

where the moment $\langle \Psi, g \rangle$ is defined as

$$\langle \Psi, g \rangle = \int_{R \times R^K} \Psi g \, d\Xi,$$

$d\Xi = dv \, d\xi_1 \cdots d\xi_K$, and the moment function vector Ψ is given by

$$\Psi = \left[1, v, \frac{v^2 + \xi^2}{2}\right]^{\mathrm{T}}. \tag{10}$$

Fortunately, for a general equation of state (4), the Euler equations (1) can be directly written in the moment form through the above Maxwell-Boltzmann distribution g and the modification of K.

In order to implement a general equation of state into the equilibrium state, we can introduce a new parameter $\tilde{\gamma}$, which satisfies the equation

$$p(\rho, e) = (\tilde{\gamma} - 1)\rho e. \tag{11}$$

As a result, the Euler equations (1) with (4) can be recovered by a Maxwell-Boltzmann distribution g in (7) with a new parameter $\tilde{K}$, defined as

$$\tilde{K} = -1 + \frac{2}{\tilde{\gamma} - 1}. \tag{12}$$

REMARK.

(a) In equations (11) and (12), $\tilde{K}$ and $\tilde{\gamma}$ are variables which depend on the macroscopic flow quantities. For an ideal gas, $\tilde{\gamma}$ and $\tilde{K}$ go to the constant as shown in equation (8).

(b) For numerical purposes, with the conservative variables $(\rho, \rho u, E)$ and equation (4), the pressure p can be written explicitly in form (11), and then get $\tilde{\gamma}$ and $\tilde{K}$.

3. BGK-TYPE SCHEMES

The BGK model for equation (1) can be written as

$$f_t + vf_x = \frac{1}{\tau}(f - g), \tag{13}$$

where f is the gas distribution function and g is the local equilibrium state given in equations (7) and (12). τ represents the particle collision time which can be a function of the local macroscopic flow variables. Due to the conservation property in particle collisions, f and g satisfy the compatibility condition

$$\int (f - g)\Psi \, d\Xi = 0, \qquad \forall x, t. \tag{14}$$

The numerical discretization of the BGK model is based on its integral solution

$$f\left(x_{j+1/2}, t, v, \xi\right) = \frac{1}{\tau}\int_0^t g\left(x', t', v, \xi\right) e^{-(t-t')/\tau}\, dt' + e^{-t/\tau} f_0\left(x_{j+1/2} - vt\right), \tag{15}$$

where $x_{j+1/2}$ is the cell interface and $x' = x_{j+1/2} - v(t - t')$ the particle trajectory. There are two unknowns in equation (15), i.e., the initial gas distribution function f_0 at time $t = 0$ and the equilibrium g in both space and time locally around $(x_{j+1/2}, t = 0)$.

Following the idea in [9–11], the BGK-type scheme for solving the Euler equations (1) with a general equation of state, along with compatibility condition (14), is described as follows.

STEP I. Use van Leer's techniques [22] to interpolate the conservative variables U_j in each cell, and get the new initial data

$$\bar{U}_j(x) = U_j\left(x_j\right) + L\left(s_j^+, s_j^-\right)\left(x - x_j\right), \qquad \forall x \in \left[x_{j-1/2}, x_{j+1/2}\right], \tag{16}$$

where $L(s_j^+, s_j^-)$ is an approximate slope of U at the grid point x_j. For example,

$$L\left(s_j^+, s_j^-\right) = \left(\operatorname{sign}\left(s_j^+\right) + \operatorname{sign}\left(s_j^-\right)\right)\frac{\left|s_j^+\right|\left|s_j^-\right|}{\left|s_j^+\right| + \left|s_j^-\right|},$$

where $s_j^{\pm} = (U_{j\pm1} - U_j)/(x_{j\pm1} - x_j)$.

STEP II. Based on the constructed data in Step I, around each cell interface $x_{j+1/2}$, the initial gas distribution f_0 can be obtained,

$$f_0(x) = \begin{cases} g^L\left(1 + a^L\left(x - x_{j+1/2}\right)\right), & x \le x_{j+1/2}, \\ g^R\left(1 + a^R\left(x - x_{j+1/2}\right)\right), & x \ge x_{j+1/2}, \end{cases} \tag{17}$$

where the status g^L and g^R are two local Maxwellian distribution functions located to the left and to the right of the cell interface $x_{j+1/2}$. The corresponding slopes $a^{L,R}$ in (17) have the form

$$a^{L,R} = \left(a_1^{L,R}, a_2^{L,R}, a_3^{L,R}\right) \cdot \Psi, \tag{18}$$

which are obtained from a Taylor expansion of the Maxwellian distribution functions. All coefficients in equation (17) can be determined from the constructed conservative variables as well as their slopes on both sides of the cell interface $x_{j+1/2}$ in Step I. We refer readers to [9] for details.

STEP III. The state g is assumed to be continuous across a cell interface, and defined by

$$g = g_0\left(1 + (1 - H[x])\bar{a}^L x + H[x]\bar{a}^R x + \bar{A}t\right), \tag{19}$$

where $H[x]$ is the Heaviside function and g_0 the equilibrium state located at ($x = x_{j+1/2}$, $t = 0$). Here $\bar{a}^{L,R}$ and $\bar{A}$ have the same form as coefficients $a^{L,R}$, which are also related to the Taylor expansion of a Maxwellian distribution functions. Taking both limits of ($x \to x_{j+1/2}, t \to 0$) in equations (15) and (19), and applying the compatibility condition (14) at ($x = x_{j+1/2}, t = 0$), g_0 can be uniquely determined in terms of f_0, i.e.,

$$U_0 \equiv \int g_0 \Psi \, d\Xi = \int_{v>0} g^L \Psi \, d\Xi + \int_{v<0} g^R \Psi \, d\Xi. \tag{20}$$

Connecting U_0 to the cell centered values $U_j(x_j)$ and $U_{j+1}(x_{j+1})$, we get three slopes for macroscopic conservative variables separately in $x > 0$ and $x < 0$, from which $\bar{a}^{L,R}$ can be obtained. Up to this point, we have obtained the initial gas distribution function f_0 and the corresponding equilibrium state g_0 at time $t = 0$.

STEP IV. Substituting equation (17) and equation (19) into equation (15), the final gas distribution function at the cell interface can be expressed as

$$\begin{aligned} f\left(x_{j+1/2}, t, u, \xi\right) &= \left(1 - e^{-t/\tau}\right) g_0 + \tau \left(\frac{t}{\tau} - 1 + e^{-t/\tau}\right) \bar{A} g_0 \\ &+ \left(\tau \left(-1 + e^{-t/\tau}\right) + t e^{-t/\tau}\right) \left(\bar{a}^L H[u] + \bar{a}^R (1 - H[u])\right) u g_0 \\ &+ e^{-t/\tau} \left(\left(1 - uta^L\right) H[u] g^L + \left(1 - uta^R\right) (1 - H[u]) g^R\right). \end{aligned} \tag{21}$$

The only unknown $\bar{A}$ in the above equation can be determined from the following three equations obtained by integrating the compatibility condition (14) in a whole CFL time step Δt at $x = x_{j+1/2}$

$$\int_0^{\Delta t} \int \left[f\left(x_{j+1/2}, t, u, \xi\right) - g\left(x_{j+1/2}, t, u, \xi\right)\right] \Psi \, d\Xi \, dt = 0.$$

There is no iteration involved from the above equation to determine A.

STEP V. Finally, the time-dependent numerical fluxes for mass, momentum, and energy across the cell interface $x_{j+1/2}$ can be obtained by taking the moments of f in (21),

$$F_{j+1/2}(t) = \int v f\left(x_{j+1/2}, t, u, \xi\right) \Psi \, d\Xi, \tag{22}$$

and the update of flow variables is based on

$$U_j^{n+1} = U_j^n - \frac{1}{\Delta x} \int_0^{\Delta t} \left(F_{j+1/2}(t) - F_{j-1/2}(t)\right) dt. \tag{23}$$

In the above algorithm, the collision time τ is used as a local constant

$$\tau = 0.05\Delta t + C_2 \Delta t \frac{|p^L - p^R|}{p^L + p^R},$$

where $C_2 = 1$ is fixed in the following numerical calculations.

4. NUMERICAL RESULTS

In this section, we present some numerical experiments to demonstrate the performance of the second order accurate BGK-type scheme presented in the last section for the Euler equations with a general equation of state. In all examples, uniform grids are used in the computational domain $0 \le x \le 1$.

Three different forms of equation of state are used in the simulation:

(a) polytropic ideal gas

$$p = (\gamma - 1)\rho e; \tag{24}$$

(b) stiffened model [13]

$$p = B\left(\frac{\rho}{\rho_0} - 1\right) + (\gamma - 1)\rho e, \tag{25}$$

where B is a constant, ρ_0 represents a reference density; and

(c) Osborne model [13,19]

$$p = \frac{1}{\rho_0 e + \psi_0}\left\{\zeta\left(a_1 + a_2|\zeta|\right) + \rho_0 e\left[b_0 + \zeta\left(b_1 + b_2\zeta\right) + \rho_0 e\left(c_0 + c_1\zeta\right)\right]\right\}, \tag{26}$$

where $\zeta = \rho/\rho_0 - 1$ and constants ρ_0, a_1, a_2, b_0,b_1, b_2, c_0, c_1, and ψ_0 depend on the material in question.

The first problem is about shock reflection in one-dimensional case for the above three equations of state.

In the computational domain, the initial conditions are

$$\rho = \rho_0, \qquad u = -u_0, \qquad e = e_0, \qquad \text{and} \qquad p = p\left(\rho_0, e_0\right). \tag{27}$$

The boundary at $x = 0$ is a rigid wall, where reflection boundary condition is imposed. This problem is about a shock reflection from the left wall. Here, γ is equal to 5/3 in all cases.

Figures 1–6 show the results from the above initial conditions and with different equations of state. For ideal and stiffened one, we take $\rho_0 = 1$, $u_0 = 1$, and $B = 1.0$. For the Osborne model, we take

$$\begin{aligned} &\rho_0 = 8.9, && a_1 = 4.9578, && a_2 = 3.6884, \\ &b_0 = 7.4727, && b_1 = 11.519, && b_2 = 5.5251, \\ &c_0 = 0.39493, && c_1 = 0.52883, && \psi_0 = 3.6, \end{aligned} \tag{28}$$

and $u_0 = 1$. In all cases, the ratio of pressure jump across the shock front takes either 10 or 2. From Figures 1–6, we observe that shock waves are sharply resolved with two interior points on the uniform grid and the correct locations of shock front have been captured for all three forms of equation of state. In these figures, solid lines denote the exact solutions, while points are numerical solutions obtained by the present scheme with 200 grid points. Our results are comparable with those from other schemes, i.e., [13].

The next three problems we consider are one-dimensional shock-tube problem for an ideal gas with the initial data

$$(\rho, u, E)_{t=0} = \begin{cases} (1, 0, 2.5), & x < 0.5, \\ (0.125, 0, 0.25), & x > 0.5, \end{cases} \tag{29}$$

$$(\rho, u, E)_{t=0} = \begin{cases} (0.445, 0.311, 8.928), & x < 0.5, \\ (0.5, 0, 1.427), & x > 0.5, \end{cases} \tag{30}$$

and

$$(\rho, u, E)_{t=0} = \begin{cases} (1, -2, 3), & x < 0.5, \\ (1, 2, 3), & x > 0.5. \end{cases} \tag{31}$$

In these problems, $\gamma = 1.4$ is used. The numerical results with uniform 200 grid points are shown in Figures 7–9. The solid lines in Figures 7 and 8 are the exact solutions of a Riemann problem which include shock wave, contact discontinuity, and rarefaction fan. The solid lines in Figure 9 are obtained from the same kinetic scheme with uniform 2000 grid points. These three problems

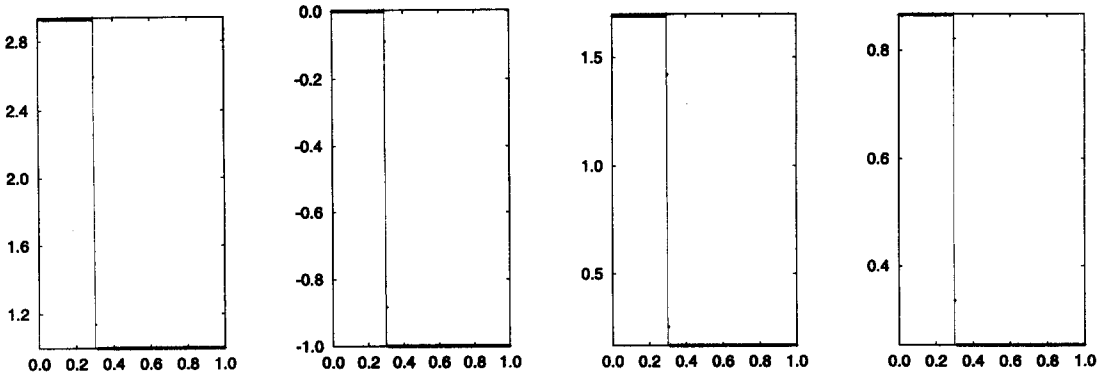

(a) Density. (b) Velocity. (c) Pressure. (d) Internal energy.

Figure 1. A shock reflection problem for γ-gas law with the pressure ratio 10. The numerical solution at $t = 0.579$ is obtained with 200 points. The solid line is the exact solution.

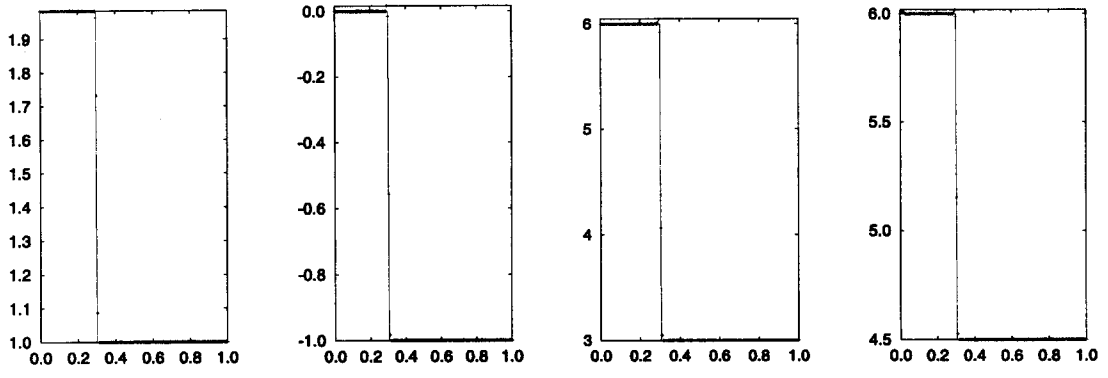

Figure 2. Same as Figure 1 with the pressure ratio 2. $t = 0.151$.

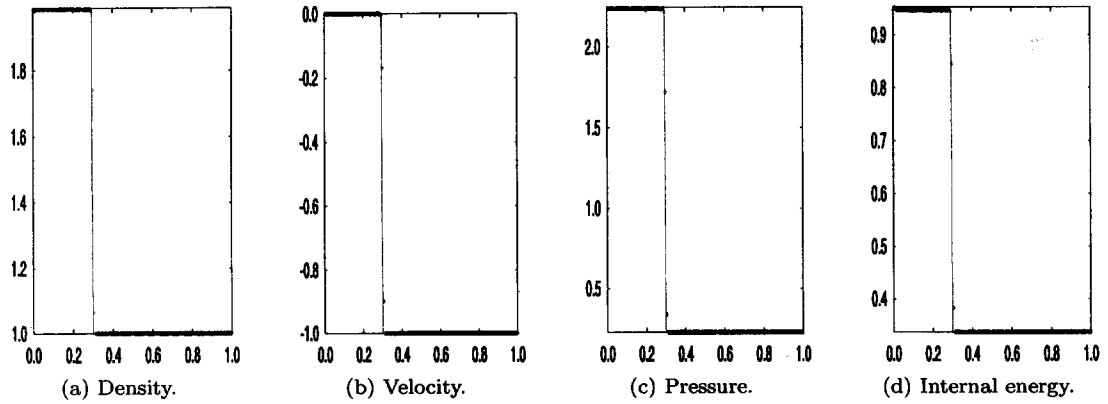

(a) Density. (b) Velocity. (c) Pressure. (d) Internal energy.

Figure 3. A shock reflection problem for stiffened model with the pressure ratio 10. The numerical solution at $t = 0.295$ is obtained with 200 points. The solid line denotes the exact solution.

have been considered as the benchmark problems for an ideal gas to demonstrate the performance of various schemes (see [9] and references therein).

The next three problems are one-dimensional shock-tube problems for the stiffened model with the initial data

$$(\rho, u, p)_{t=0} = \begin{cases} (1, 0, 8), & x < 0.5, \\ (0.125, 0, 0.1), & x > 0.5, \end{cases} \tag{32}$$

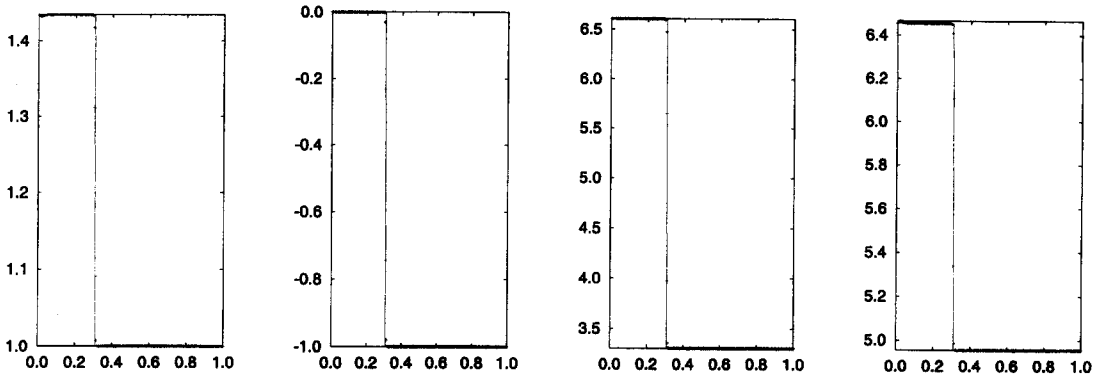

Figure 4. Same as Figure 3 with the pressure ratio 2. $t = 0.130$.

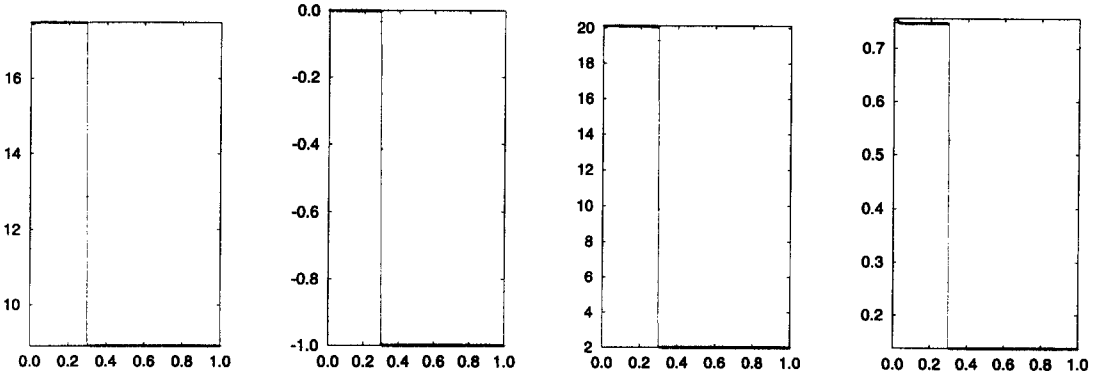

(a) Density. (b) Velocity. (c) Pressure. (d) Internal energy.

Figure 5. A shock reflection problem for Osborne model with the pressure ratio 10. The numerical solution at $t = 0.288$ is obtained with 200 points. The solid line is the exact solution.

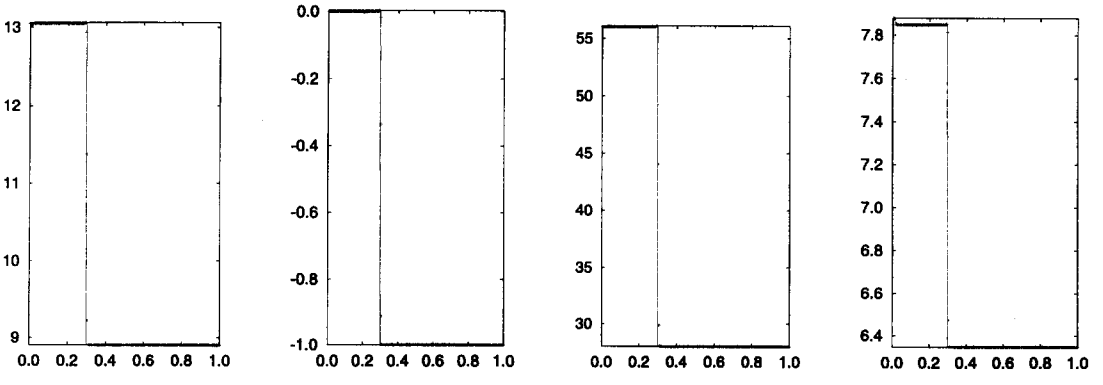

Figure 6. Same as Figure 5 with the pressure ratio 2. $t = 0.139$.

$$(\rho, u, p)_{t=0} = \begin{cases} (0.8, 0, 10), & x < 0.5, \\ (1, 0, 0.1), & x > 0.5, \end{cases} \tag{33}$$

and

$$(\rho, u, p)_{t=0} = \begin{cases} (1, -2, 8), & x < 0.5, \\ (1, 2, 8), & x > 0.5. \end{cases} \tag{34}$$

In these problems, $\gamma = 1.4$, $B = 1.0$, and $\rho_0 = 1$ are used. The numerical solutions are shown in Figures 10–12. The "exact" solutions (solid lines) are obtained by the same scheme with uniform 2000 points. The wave structures in Figures 10–12 are quite similar to the ideal case in Figures 7–9. We observe that shock waves are resolved very well, but there is slight numerical

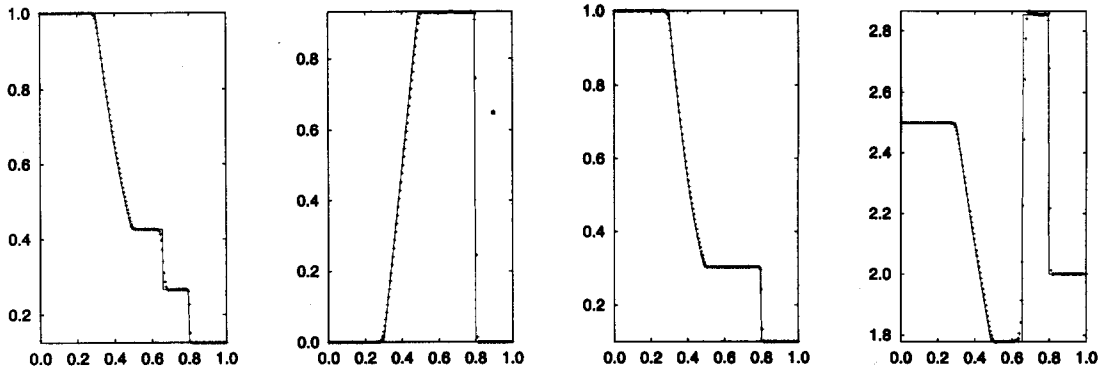

(a) Density. (b) Velocity. (c) Pressure. (d) Internal energy.

Figure 7. Problem of equation (29). The solutions at $t = 0.17$ are obtained with 200 points.

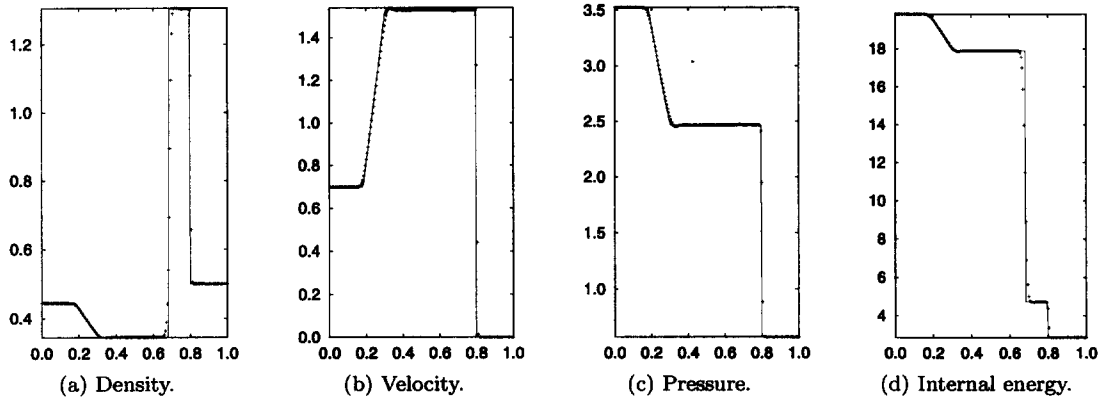

(a) Density. (b) Velocity. (c) Pressure. (d) Internal energy.

Figure 8. Problem of equation (30). The solutions at $t = 0.12$ are obtained with 200 points.

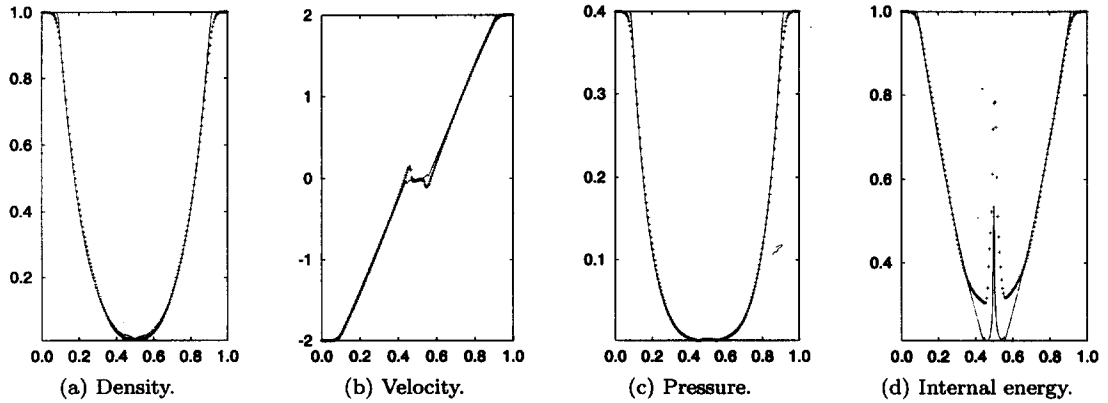

(a) Density. (b) Velocity. (c) Pressure. (d) Internal energy.

Figure 9. Problem of equation (31). The solutions at $t = 0.15$ are obtained with 200 points.

undershoot for velocity at the contact surface in Figure 11. The main reason for it is that the large temperature difference at the contact surface and the stiffness of the equation of state. This phenomenon usually happens in the ideal cases too in many shock capturing schemes.

The final three problems we consider are one-dimensional shock-tube problem for Osborne model with the initial data

$$(\rho, u, e)_{t=0} = \begin{cases} (1, 0, 7.22E + 6), & x < 0.5, \\ (0.05, 0, 1.44E + 6), & x > 0.5, \end{cases} \tag{35}$$

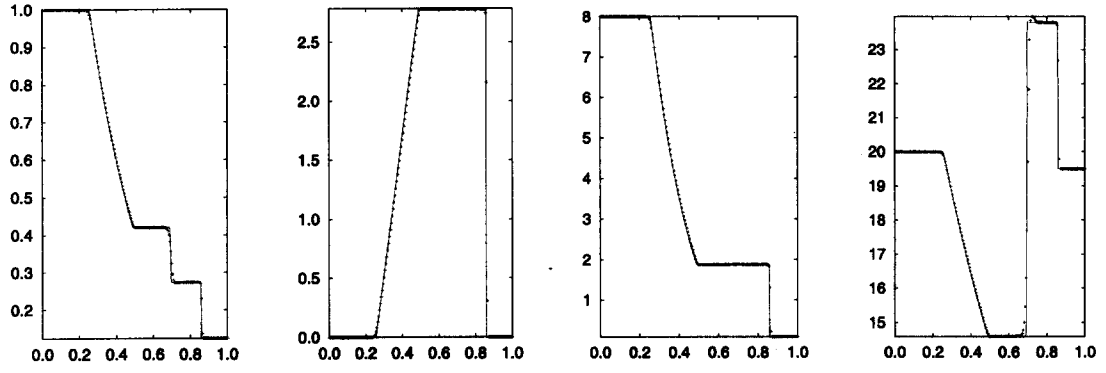

(a) Density. (b) Velocity. (c) Pressure. (d) Internal energy.

Figure 10. Problem of equation (32). The solutions at $t = 0.075$ are obtained with 200 points.

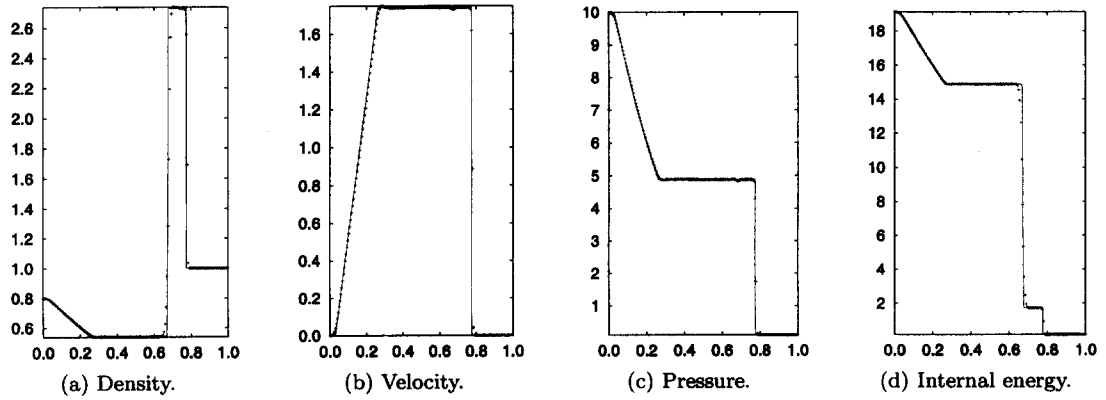

(a) Density. (b) Velocity. (c) Pressure. (d) Internal energy.

Figure 11. Problem of equation (33). The solutions at $t = 0.1$ are obtained with 200 points.

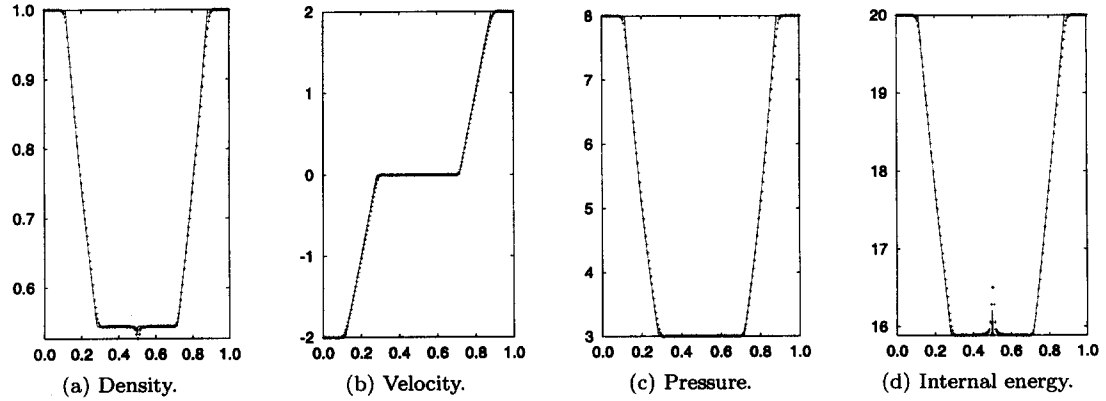

(a) Density. (b) Velocity. (c) Pressure. (d) Internal energy.

Figure 12. Problem of equation (34). The solutions at $t = 0.07$ are obtained with 200 points.

$$(\rho, u, e)_{t=0} = \begin{cases} (0.066, 0, 7.22E+6), & x < 0.5, \\ (0.03, 0, 1.44E+6), & x > 0.5, \end{cases} \tag{36}$$

and

$$(\rho, u, e)_{t=0} = \begin{cases} (0.1, -2, 1.44E+6), & x < 0.5, \\ (0.1, 2, 1.44E+6), & x > 0.5. \end{cases} \tag{37}$$

In these problem, the parameters in the equation of state take the following values:

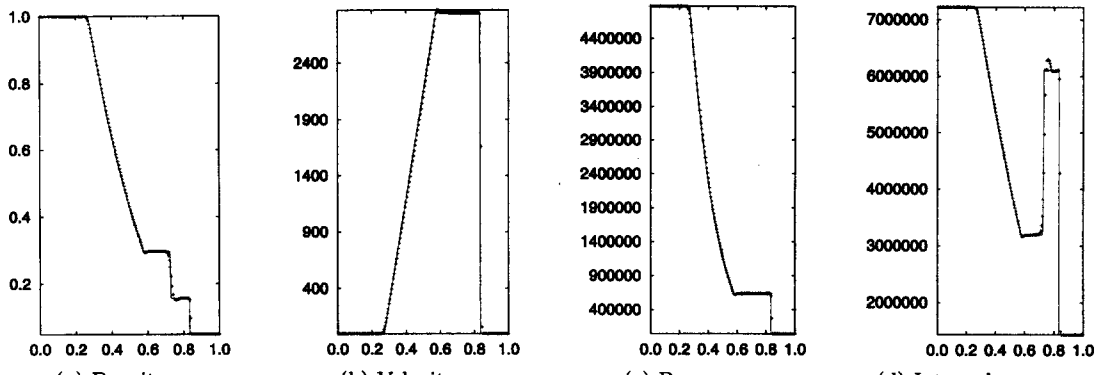

(a) Density. (b) Velocity. (c) Pressure. (d) Internal energy.

Figure 13. Problem of equation (35). The solutions at $t = .8E-4$ are obtained with 200 points.

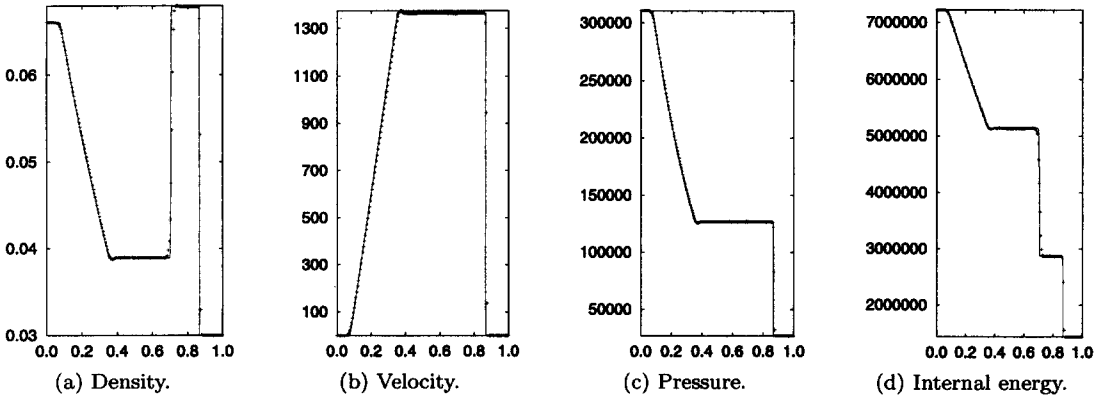

(a) Density. (b) Velocity. (c) Pressure. (d) Internal energy.

Figure 14. Problem of equation (36). The solutions at $t = 1.5E-4$ are obtained with 200 points.

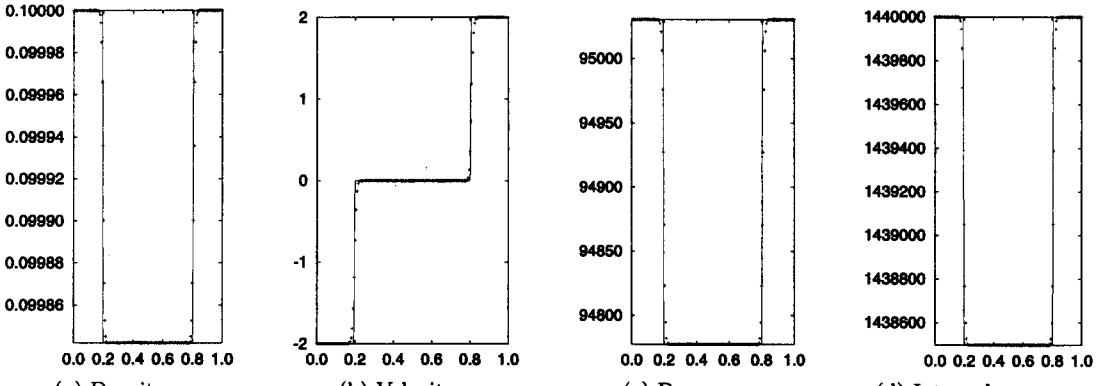

(a) Density. (b) Velocity. (c) Pressure. (d) Internal energy.

Figure 15. Problem of equation (37). The solutions at $t = 2.4E-4$ are obtained with 200 points.

$$\begin{aligned} &\rho_0 = 0.01, && a_1 = 3.84E-4, && a_2 = 1.756E-3, \\ &b_0 = 1.312E-2, && b_1 = 6.256E-2, && b_2 = 0.2133, \\ &c_0 = 0.5132, && c_1 = 0.6761, && \psi_0 = 2.E-2, \end{aligned} \tag{38}$$

and $\gamma = 5/3$. The numerical and "exact" solutions (solid lines) are given in Figures 13–15. The "exact" solutions are obtained by the same kinetic scheme with uniform 2000 grid points. The present scheme captures important wave structures such as a rarefaction wave, a contact discontinuity and a shock wave under the Osborne model in Figures 13 and 14. Two steep

rarefaction waves are also accurately obtained in Figure 15. Although the form of the equation of state is very complex, shock waves are sharply resolved with two interior cells. Also, we observe that our numerical solutions obtained on different mesh sizes are consistent.

5. CONCLUSION

In this paper, we have translated a general equation of state into a new definition of internal degree of freedom in the Maxwell-Boltzmann distribution function of an equilibrium state, from which the Euler equations for real gases can be recovered. Based on the kinetic model, we have extended the BGK-type finite volume scheme to solve the Euler equations with general equation of state. This new scheme has been applied to three expressions of the equation of state. There is no derivative calculation of the pressure law in the flux evaluation. The above scheme is tested on one-dimensional shock reflection and shock-tube problems. The numerical results demonstrate the validity of the extension of the kinetic scheme and the accuracy of the scheme in the simulation of real gases.

REFERENCES

1. S.Y. Chou and D. Baganoff, Kinetic flux-vector splitting for the Navier-Stokes equations, *J. Comput. Phys.* **130** (2), 217–230 (1997).
2. J.C. Mandal and S.M. Deshpande, Kinetic flux vector splitting for Euler equations, *Computers and Fluids* **23** (2), 447–478 (1994).
3. J.M. Moschetta and D.I. Pullin, A robust low diffusive kinetic scheme for the Navier-Stokes/Euler equations, *J. Comput. Phys.* **133** (2), 193–204 (1997).
4. B. Perthame, Second-order Boltzmann schemes for compressible Euler equations in one and two space dimensions, *SIAM J. Numer. Anal.* **29** (1), 1–29 (1992).
5. K.H. Prendergast and K. Xu, Numerical hydrodynamics from gas-kinetic theory, *J. Comput. Phys.* **109** (1), 53–66 (1993).
6. D.I. Pullin, Direct simulation methods for compressible inviscid ideal gas flow, *J. Comput. Phys.* **34** (2), 231–244 (1980).
7. K.S. Ravichandran, Higher order KFVS algorithms using compact upwind difference operators, *J. Comput. Phys.* **130** (2), 161–173 (1997).
8. R.D. Reitz, One-dimensional compressible gas dynamics calculations using the Boltzmann equations, *J. Comput. Phys.* **42** (1), 108–123 (1981).
9. K. Xu, Gas-kinetic schemes for unsteady compressible flow simulations, Presented at the *29th CFD, Lecture Series 1998-03, von Karman Institute for Fluid Dynamics, February 23–27, 1998.*
10. K. Xu, L. Martinelli and A. Jameson, Gas-kinetic finite volume methods, flux-vector splitting and artificial diffusion, *J. Comput. Phys.* **120** (1), 48–65 (1995).
11. K. Xu and K.H. Prendergast, Numerical Navier-Stokes solutions from gas-kinetic theory, *J. Comput. Phys.* **114** (1), 9–17 (1994).
12. P. Colella and H.M. Glaz, Efficient solution algorithms for the Riemann problem for real gases, *J. Comput. Phys.* **59** (2), 264–289 (1985).
13. P. Glaister, An approximate linearised Riemann solver for the Euler equations for real gases, *J. Comput. Phys.* **74** (2), 382–408 (1988).
14. P. Glaister, An efficient numerical method for compressible flows of a real gas using arithmetic averaging, *Computers Math. Applic.* **28** (7), 97–113 (1994).
15. W. Walters, Analysis of flux-split algorithms for Euler's equations with real gases, *AIAA J.* **27** (5), 524–531 (1989).
16. M.S. Liou, B. van Leer and J.S. Shuen, Splitting of inviscid fluxes for real gases, *J. Comput. Phys.* **87** (1), 1–24 (1990).
17. M. Vinokur and J.L. Montagne, Generalized flux-vector splitting and Roe average for an equilibrium for real gas, *J. Comput. Phys.* **89** (2), 276–300 (1990).
18. F. Coquel and B. Perthame, Relaxation of energy and approximate Riemann solvers for general laws in fluid dynamics equations, *SIAM J. Numer. Anal.* **35** (6), 2223–2249 (1998).
19. P. Montarnal and C.W. Shu, Real gas computation using an energy relaxation method and high-order WENO schemes, *J. Comput. Phys.* **148** (1), 59–80 (1998).
20. C. Cercignani, *The Boltzmann Equation and Its Applications*, Springer-Verlag, (1988).
21. S. Chapman and T.G. Cowling, *The Mathematical Theory of Non-Uniform Gases*, Third Edition, Cambridge University Press, (1990).
22. B. van Leer, Towards the ultimate conservative difference schemes V. A second-order sequal to Godunov's method, *J. Comput. Phys.* **32** (1), 101–136 (1979).